Stochastic analysis of exit fluid temperature records from the active TAG hydrothermal mound (Mid-Atlantic Ridge, 26°N): 1. Modes of variability and implications for subsurface flow

R. A. Sohn[1]

Received 8 April 2006; revised 15 February 2007; accepted 21 March 2007; published 11 July 2007.

[1] Yearlong time series records of exit fluid temperature from the active TAG hydrothermal mound (Mid-Atlantic Ridge, 26°N) reveal a complex space-time pattern of flow variability within the mineral deposit. Exit fluid temperatures were measured every 8–10 min from 17 sites distributed across the upper terrace of the mound from June 2003 to June 2004. High-temperature records were obtained using Deep Sea Power and Light SeaLogger® probes deployed in fractures discharging ~360°C black smoker fluids, and low-temperature records were obtained using VEMCO Ltd. Minilog probes deployed in cracks discharging ~20°C diffuse flow fluids. The temperature records are considerably more variable than those acquired from vent fields on the fast spreading East Pacific Rise and exhibit a complex mix of both episodic and periodic variability. The diffuse flow records alternate between periods of discharge and periods of what I infer to be recharge when fluid temperatures are equal to background water column levels (~2.7°C) as ambient seawater is drawn into the seafloor. The space-time patterns of these episodic variations suggest that they represent reorganizations of the secondary circulation system driving diffuse discharge on the upper terrace of the mound on timescales from a few hours to a few days, most likely in response to permeability perturbations. Harmonic temperature oscillations were observed over a range of periods, with the principal lunar semidiurnal tidal period (M2) being most dominant. During certain times, exit fluid temperatures at diffuse sites pulse at diurnal and semidiurnal tidal periods when they are hovering near background water column levels, which I interpret as flow reversals associated with the vertical displacement of a fluid boundary layer at the seafloor interface when the local net flux is near zero. The pulsing behavior is predicted by poroelastic models of tidal loading but is not consistent with effects from tidal currents, which demonstrates that poroelastic effects from tidal loading modulate shallow subsurface flow at the active TAG mound.

Citation: Sohn, R. A. (2007), Stochastic analysis of exit fluid temperature records from the active TAG hydrothermal mound (Mid-Atlantic Ridge, 26°N): 1. Modes of variability and implications for subsurface flow, *J. Geophys. Res.*, *112*, B07101, doi:10.1029/2006JB004435.

1. TAG Hydrothermal Field and Active Mound

[2] The temporal variability of exit fluids discharged at deep-sea vent fields provides important information regarding the hydrogeology and subsurface circulation patterns of hydrothermal flow in young oceanic crust. Spectral methods have been used to show that tidal processes play modulate exit fluid properties [e.g., *Chevaldonne et al.*, 1991; *Kinoshita et al.*, 1996; *Pruis and Johnson*, 2004; *Schultz et al.*, 1996; *Tivey et al.*, 2002], which may reflect either a poroelastic response to tidal loading [e.g., *Crone and Wilcock*, 2005; *Jupp and Schultz*, 2004; *Wang and Davis*, 1996], an interface (e.g., Bernoulli) effect from tidal currents [e.g., *Tivey et al.*, 2002], or perhaps a combination of both. It has also been observed that exit fluid time series records commonly contain abrupt variations apparently related to subsurface perturbations, and in some cases these perturbations have been associated with specific geological events, such as volcanic eruptions [*Baker et al.*, 1999] or earthquakes [*Davis et al.*, 2004; *Johnson et al.*, 2000; *Sohn et al.*, 1998].

[3] Periodic variability at tidal frequencies and episodic variability related to geological processes appear to be common features for exit fluid time series records acquired from deep-sea vent fields, but the nature of variations varies with geographical and geological setting. Fluid dynamics in the water column above a mid-ocean ridge (MOR) depend on the position of the vent field with respect to the basin-scale tidal response, and also with respect to the Earth's

[1]Woods Hole Oceanographic Institution, Woods Hole, Massachusetts, USA.

0148-0227/07/2006JB004435$09.00

inertial system. The exact nature of tidal pressures and currents at a vent field also depends on the spreading center topography. The interaction of barotropic tidal currents with rough topography at ridges can generate turbulence that blue shifts perturbations toward higher frequencies [e.g., *Polzin et al.*, 1997], and the basic rotary structure of open ocean tidal currents can be modified to elliptical patterns (with the major axis oriented along the ridge strike) within the confines of the axial valley formed at intermediate to slow spreading rates [e.g., *Tivey et al.*, 2002]. We may therefore expect to observe a range of tidal behaviors in exit fluid time series data from different sites along the global MOR system.

[4] Similarly, the nature of episodic perturbations to hydrothermal flow depends on the geological context of the vent field. Fast spreading MORs have more frequent episodes of diking and volcanism that may perturb the thermal and stress states of the elastic medium hosting hydrothermal convection [e.g., *Cherkaoui et al.*, 1997; *Rubin*, 1992] but typically lack a sufficiently thick brittle layer to allow for the generation of large earthquakes [e.g., *Huang and Solomon*, 1988; *Sohn et al.*, 1999]. By contrast, slow spreading MORs have much more infrequent episodes of magmatism, but they typically have a thick brittle layer that can generate large earthquakes ($M_w \geq 4$) [e.g., *Huang and Solomon*, 1988] with correspondingly large stress and permeability perturbations to the flow medium. In addition, tectonized slow spreading ridges may have high-permeability fault systems that focus hydrothermal discharge to discrete portions of the seafloor over long periods of time thereby allowing for the deposition of massive hydrothermal deposits [e.g., *Wilcock and Delaney*, 1996]. These large deposits have their own internal set of dynamics related to mineralization/dissolution and hydraulics that may play an important role in triggering episodic variability in exit fluid parameters. We therefore expect to observe a range of episodic behaviors in exit fluid time series data from geologically disparate sites along the global MOR system.

[5] We can use both periodic (i.e., tidal) and episodic modes of variability in hydrothermal exit fluid time series data to constrain subsurface flow, but unfortunately the number of long-term flow records available for analysis has been limited to only a few vent fields owing to logistical issues associated with acquiring the data. Field campaigns to acquire hydrothermal flow records over statistically significant time intervals have largely been limited to the fast spreading East Pacific Rise (EPR) in the 9°–10°N region [e.g., *Scheirer et al.*, 2006; *Von Damm et al.*, 2005], and a few discrete segments of the intermediate spreading Juan de Fuca Ridge (JdFR) [e.g., *Davis et al.*, 2004; *Johnson et al.*, 2000; *Tivey et al.*, 2002]. To this point flow records from massive hydrothermal deposits on tectonically dominated slow spreading ridges have been limited to short observation periods of 1–2 weeks [*Fujioka et al.*, 1997; *Kinoshita et al.*, 1996; *Schultz et al.*, 1996], and as a result we do not understand how hydrothermal circulation responds to these high seismicity rate environments, nor how the internal dynamics of massive mineral deposits affect shallow subsurface flow.

[6] In this paper I present the results of a yearlong exit fluid temperature monitoring campaign at the TAG (Trans-Atlantic Geotraverse) active hydrothermal mound, a massive sulfide deposit on the slow spreading Mid-Atlantic Ridge (MAR) at ~26°N [*Rona*, 1980]. I begin by providing an overview of the hydrogeological setting of the TAG field and then describe the experiment and the periodic and episodic modes of variability observed in both high-temperature (black smoker) and low-temperature (diffuse) flow records. I use these results to make inferences regarding flow patterns in the shallow subsurface regime, and conclude by discussing the results in the context of a synoptic model for hydrothermal circulation in the region. A stochastic signal model for the episodic modes of variability observed in the diffuse flow records using probabilistic functions of Markov chains is described in the companion paper [*Sohn*, 2007].

2. TAG Field and the Exit Fluid Temperature Monitoring Experiment

[7] The TAG hydrothermal field (Figure 1) is located on the Mid-Atlantic Ridge (MAR) at ~26°N [e.g., *Rona*, 1980]. The field is composed of six (known) high-temperature sulfide deposits [e.g., *Rona et al.*, 1993] scattered along the hanging wall of a long-lived normal fault [e.g., *deMartin et al.*, 2007; *Tivey et al.*, 2003]. A low-temperature, Mn and Fe-Mn oxide zone has also been found partway up the footwall of the eastern, valley-forming normal fault [*Rona et al.*, 1993, 1998]. The TAG field has been venting high-temperature fluids for at least ~140,000 years [*Lalou et al.*, 1998; *You and Bickle*, 1998], with the locus of discharge switching between the various high-temperature deposits, possibly with some overlap, at apparently random intervals. Individual mounds in the field compare in size to the Solea ore fields in Cyprus [*Humphris and Cann*, 2000].

[8] Present-day high-temperature discharge is focused at the active TAG mound, a massive (~3.9 million ton) sulfide deposit with a surface expression roughly the size of a major sporting stadium. In plan view the active mound consists of two circular terraces, each about 20 m tall (Figure 2), with a ~100 m diameter upper terrace overlying a ~200 m diameter lower terrace. The upper terrace is capped by a ~12 m tall anhydrite "cone" (dark gray triangle in Figure 2), on top of which sits the main sulfide chimney. The region around the anhydrite cone and main chimney is densely colonized by vent endemic macrofaunal communities [e.g., *Gebruk et al.*, 1997; *Van Dover et al.*, 1998] and has previously been referred to as the "black smoker complex" [e.g., *Goto et al.*, 2003].

[9] We deployed 21 exit fluid temperature probes on the upper terrace of the active TAG mound (Figure 2) using the DSRV *Alvin* in June 2003 as part of a multidisciplinary experiment to study the relationship between seismicity and fluid flow. Visible modes of hydrothermal discharge (i.e., black smoker venting and shimmering, diffuse flow) were limited to the upper terrace of the mound during our dive programs in 2003 and 2004. Sites of vigorous discharge included the Ocean Drilling Program (ODP) 6 depression, cracks along the perimeter of the upper terrace, and some discrete, point source, features at sites within the flat-lying region near ODP reentry cones (Figure 2). The "Kremlin" area on the south side of the lower terrace, which hosted 250–300°C discharge in 1988 [*Campbell et al.*, 1988; *Thompson et al.*, 1988], was inactive during our dive

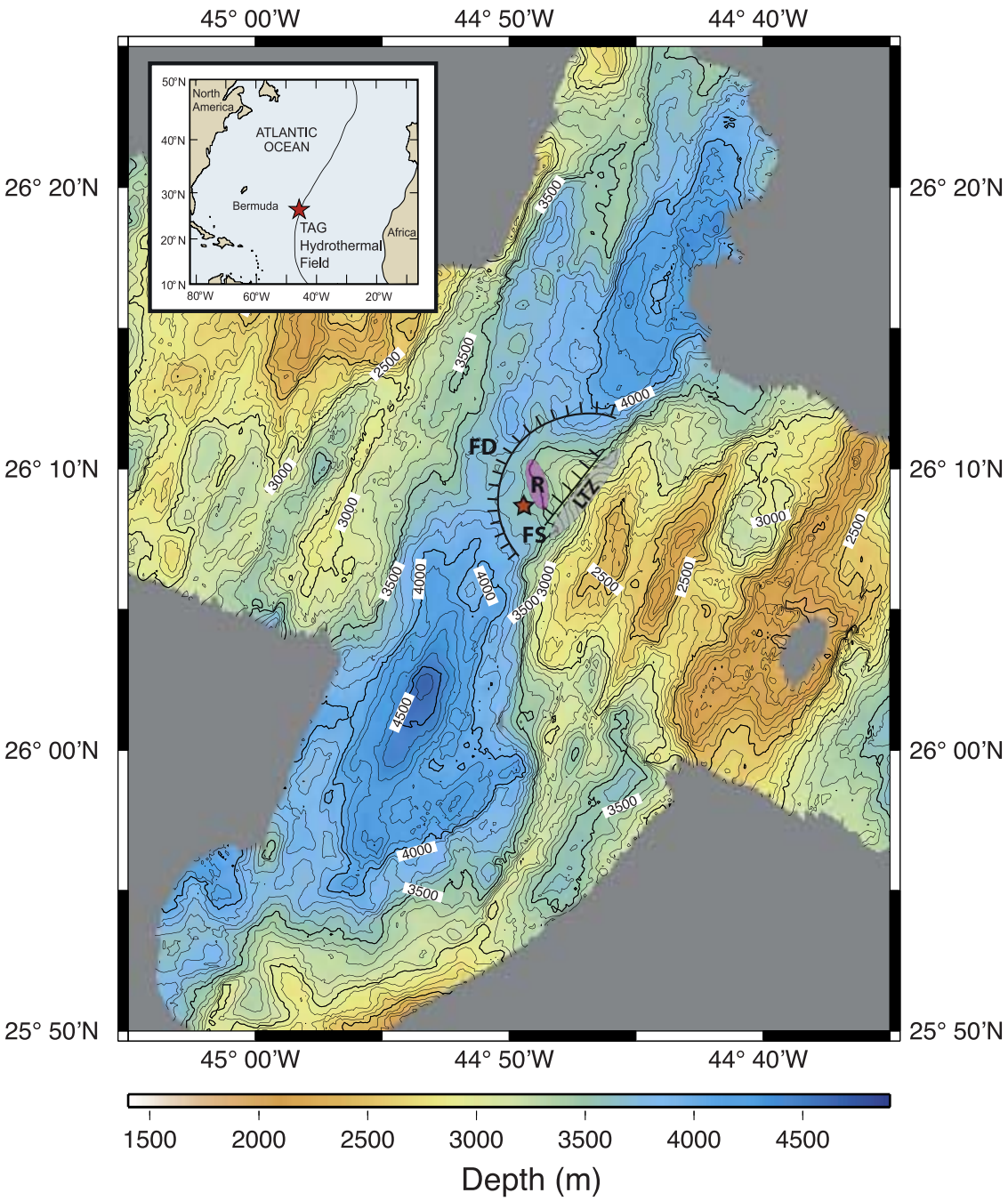

Figure 1. Color-coded bathymetric map (100 m contour intervals) of the Mid-Atlantic Ridge at 26°N with primary hydrogeologic features of the TAG hydrothermal field. Extension on the east side of the axial valley is accommodated on a long-lived, dome-shaped, detachment fault. The subsurface position of the fault deep within the crust (as defined by active seismicity [*deMartin et al.*, 2007]) is shown with the hatched line labeled "FD", and the approximate intersection of the fault with the seafloor (as defined by dive observations [*Zonenshayn et al.*, 1989] and near-bottom magnetics [*Tivey et al.*, 2003]) is shown with the hatched line labeled "FS". The seafloor intersection of the fault is not well constrained and is not necessarily a straight line, as drawn here for simplicity. The active TAG mound is shown with a red star, and the relict high-temperature mounds are shown with a violet ellipse labeled "R" [*Rona et al.*, 1993, 1984]. Low-temperature alteration has been observed in patchy regions within the gray-shaded ellipse labeled "LTZ" [*Rona et al.*, 1993]. The location of the hydrothermal field in the Atlantic Ocean is shown in the inset.

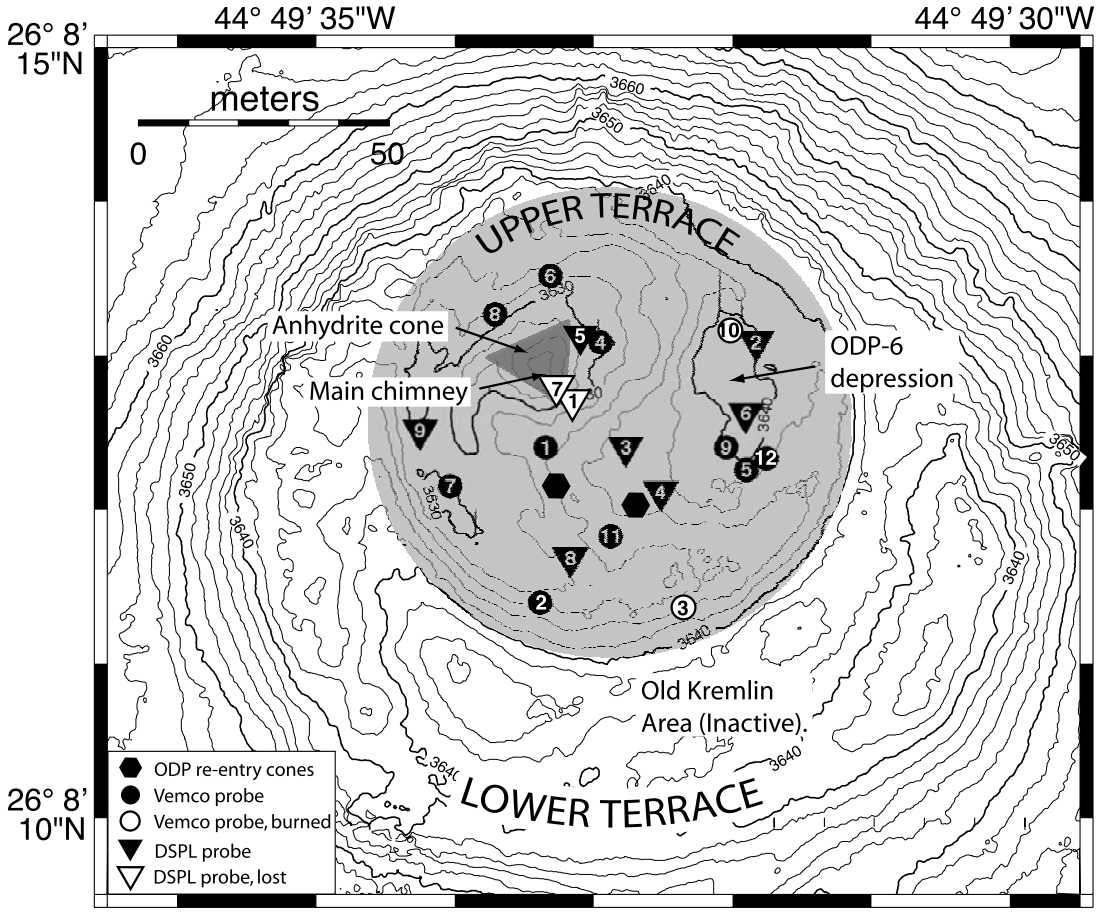

Figure 2. Temperature probe locations and structural features of the active TAG mound superimposed on microbathymetric data (2 m contour spacing) from *Roman et al.* [2005]. All of the probes were deployed on the upper terrace of the mound, which is labeled and designated by the light gray shaded circle. The lower terrace spans most of this figure window and is also labeled. High-temperature discharge is focused at the central black smoker complex, which consists of large (~8 m tall) main chimney that sits atop a broad cone of anhydrite (dark gray triangle). Temperature probe locations and status upon recovery are given in the legend.

programs in 2003 and 2004, as was the lower terrace of the mound, as a whole.

[10] High-temperature (black smoker) records were obtained using Deep Sea Power and Light (DSPL, San Diego, California) SeaLogger® probes, and low-temperature (diffuse venting) records were obtained using VEMCO (VEMCO Ltd., Nova Scotia, Canada) Minilog probes [*Fornari et al.*, 1994, 1996]. The high-temperature probes were deployed in cracks and chimneys venting black smoke. The low-temperature probes were mounted on plastic wands (in pairs for redundancy) and lodged into cracks venting shimmering water. Digital images of sample probe deployments (frame grabs of *Alvin* dive video) are shown in Figure 3. We note that it was not possible to deploy probes within the main chimney, itself, because it was enshrouded in black smoke and could not be approached with the submersible.

[11] The probes were recovered 17 months later in November 2004 using the ROV *Jason 2*. Two of the high-temperature probes (H1, H7) could not be found during recovery, and appear to have been buried and lost in a chimney collapse/debris slide event. All of the other probes were recovered, but no data was obtained from low-temperature probes L3 and L10 because they were destroyed (burned) when the pressure housings were exposed to high-temperature fluids during the deployment. All of the probes were recovered in their original position and orientation except for low-temperature probe L2, which was toppled over and appears to have been knocked down 11–16 days into the deployment (based on inspection of the data records). In total, we obtained 17 complete data records, 16 of which are from undisturbed deployments, over the interval from June 2003 to June 2004 (all probes stopped recording several months before recovery when the data buffers became full).

[12] The sampling characteristics vary somewhat for each probe type (see list in Table 1), but in general, the high-temperature probes sampled every 10 min over the temperature range from 152–460°C, and the low-temperature probes sampled every 8 min over the range from 0 to 60°C. The complete set of calibrated (using laboratory derived coefficients) exit fluid temperature time series

records are shown in Figures 4 and 5, and these data are also available for download via anonymous ftp to obslab.whoi.edu/pub/ras/STAG/Exitfluid_data.

[13] The temperature records exhibit a complex mix of episodic and harmonic variability, with large amplitude perturbations at many sites exceeding the instrument measurement range. All of the high-temperature probes clipped low (at ~150°C) during long intervals when discharge temperatures at the black smoker sites dropped more than 200°C from deployment values. Conversely, several of the low-temperature probes (L1, L2, L4, and L7) clipped high (~60°C) when discharge temperatures increased by more than 40°C from deployment values. This degree of high-amplitude variability for both black smoker and diffuse exit fluid temperatures was unexpected, and contrasts markedly with more stable records obtained from vent fields on the East Pacific Rise [e.g., *Scheirer et al.*, 2006].

[14] Histograms of the unclipped temperature records are highly skewed, long-tailed, and multipeaked (Figure 5). The multimodal character of the histograms primarily results from the fact that the records alternate between periods when fluid temperatures are equal to background bottom water values, and periods when temperatures are elevated up to anywhere from a few, to a few hundred, degrees centigrade. The data also exhibit a strong correlation between mean and variance at both instantaneous and long-term timescales (Figure 6).

3. Abrupt Temperature Perturbations, Flow Episodes, and Events

[15] Both the high- and low-temperature records exhibit episodic variability, with abrupt temperature perturbations that often occur at the beginning and/or end of flow episodes (a flow episode being defined as a period during

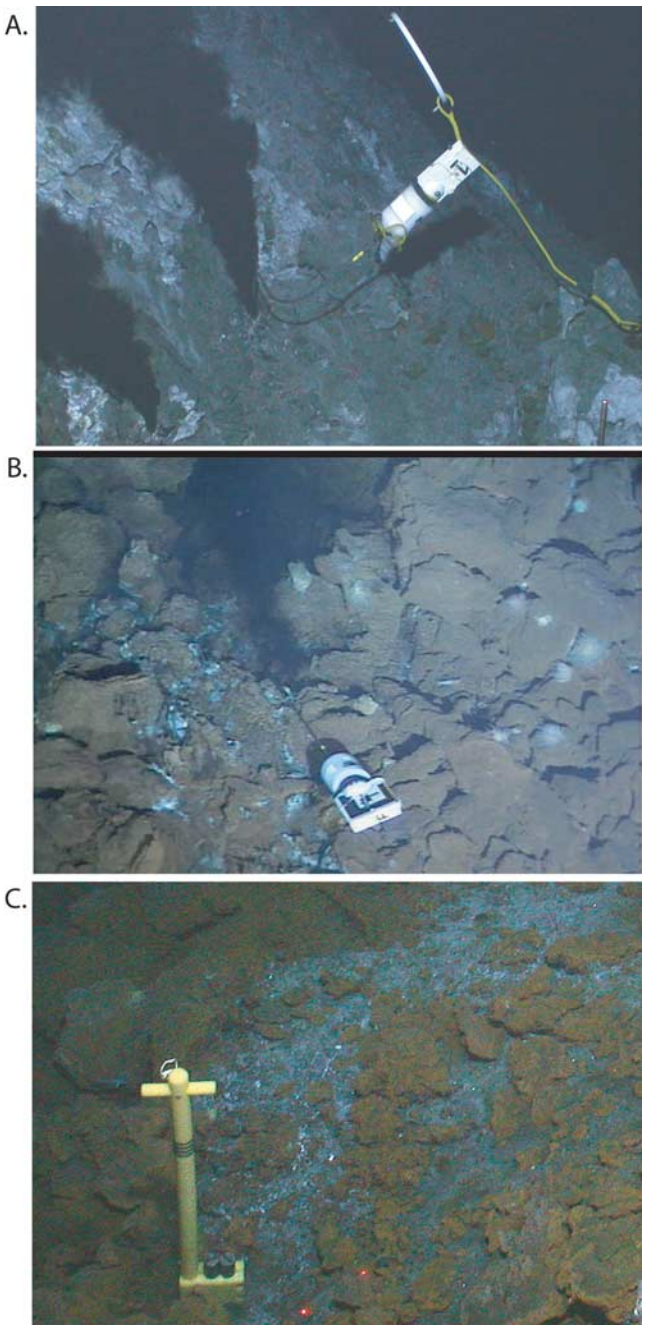

Figure 3. *Alvin* dive video digital frame grabs of sample probe deployments. (a) Example high-temperature probe deployment on anhydrite cone. Temperature measurements are made by thermocouples at the tip of the "stingers" with data loggers located in the cylindrical white housings at the far end of the probe to protect from exposure to hot fluids. Rectangular blocks of white syntactic foam were fastened to the data loggers for buoyancy compensation. High-temperature probes 1 and 5 were lanced in this way into places where black smoke was "leaking" out of the anhydrite cone. Probe 1 (shown) was lost during the deployment, presumably to a debris flow down the steep southeastern face of the cone. A bucket lid marker on a yellow polypropylene line, which was used to aid in recovery, is visible just behind the probe. (b) Example high-temperature probe deployment in a sulfide-encrusted crack on the upper terrace. High-temperature probes 2, 3, 4 (shown), 6, 8, and 9 were deployed in this way by lancing them into places where black smoke was emanating from cracks in the anhydrite substrate that had been encrusted with sulfide material. Anemones, which commonly populate regions of warm diffuse discharge, are visible on the right side of the digital image. (c) Example low-temperature probe deployment on the upper terrace. Low-temperature probes were deployed in pairs at the end of yellow mallets designed for use with the *Alvin* manipulator system. These deployment sites are essentially identical to the high-temperature sites described in Figure 3b, except the low-temperature probes were deployed along these cracks in places that were discharging shimmering (~20°C) as opposed to black smoker (~360°C) fluids at the beginning of the experiment. Low-temperature probe 4, deployed near the base of the anhydrite cone, is shown here. Note how the anhydrite substrate (white) is clearly visible beneath a thin, patchy, layer of sulfides (brownish yellow). The two red dots at the bottom of the frame are red lasers with a calibrated offset distance of 10 cm.

Table 1. Temperature Probe Fact Sheet

Probe	Type	Range, °C	Resolution, °C	Sampling Period, min	Data Start Time (Month/Day/Year, Day[a])	Data Stop Time (Month/Day/Year, Day[a])	Mean *dT*, °C	Variance,[b] °C	Percent Time Flow On
H1	DSPL	152–460	1.2	10	lost	lost	lost	lost	lost
H2	DSPL	152–460	1.2	10	06/27/03, 177	05/13/04, 497	>26.4[b]	?	>0.12[b]
H3	DSPL	152–460	1.2	10	06/27/03, 177	05/13/04, 497	>4.3[b]	?	>0.02[b]
H4	DSPL	152–460	1.2	10	06/27/03, 177	05/13/04, 497	>11.1[b]	?	>0.05[b]
H5	DSPL	152–460	1.2	10	06/27/03, 177	05/13/04, 497	>60.7[b]	?	>0.23[b]
H6	DSPL	152–460	1.2	10	06/27/03, 177	05/13/04, 497	>26.5[b]	?	>0.11[b]
H7	DSPL	152–460	1.2	10	lost	lost	lost	lost	lost
I8	DSPL	0–120	1.5	240	06/28/03, 178	04/23/04, 478	58.1	1270.7	0.99
I9	DSPL	0–120	1.5	60	06/29/03, 179	05/25/04, 509	>110.8[c]	?	1.00
L1	VEMCO	0–60	0.2	8	06/27/03,177	06/24/04, 539	0.8	9.5	0.40
L2	VEMCO	0–60	0.2	8	06/27/03,177	06/24/04, 539	knocked down	knocked down	knocked down
L3	VEMCO	0–60	0.2	8	burned	burned	burned	burned	burned
L4	VEMCO	0–60	0.2	8	06/27/03,177	06/24/04, 539	6.0	163.8	0.55
L5	VEMCO	0–60	0.2	8	06/27/03,177	06/24/04, 539	3.9	39.8	0.56
L6	VEMCO	0–60	0.2	8	06/27/03,177	06/24/04, 539	4.2	19.9	0.83
L7	VEMCO	0–60	0.2	8	06/27/03,177	06/24/04, 539	>31.7[d]	>567.6	0.93
L8	VEMCO	0–60	0.2	8	06/27/03,177	06/24/04, 539	12.4	69.5	0.97
L9	VEMCO	0–60	0.2	8	06/27/03,177	06/24/04, 539	1.0	4.8	0.27
L10	VEMCO	0–60	0.2	8	burned	burned	burned	burned	burned
L11	VEMCO	0–60	0.2	8	06/27/03,177	06/24/04, 539	4.8	16.6	0.83
L12	VEMCO	0–60	0.2	8	06/27/03,177	06/24/04, 539	0.36	2.0	0.14

[a]Days after 1 January 2003.
[b]Probes clipped low at 150°C for long periods of time, conservative estimates for mean anomaly and % time flow on were made by assuming background temperature (no anomaly) for all clipped observations. Variance estimate is not possible.
[c]Probe clipped high at 120°C for most of deployment, conservative estimate for mean anomaly made by using clipped data. Variance estimate not possible.
[d]Probe clipped high at 60°C for extended periods. Conservative, but first-order correct, estimate for mean anomaly made by using clipped data. Lower bound for variance estimated by using clipped data.

which exit fluid temperatures are elevated above background water column temperature). Although there may not be a monotonic relationship between exit fluid temperature and velocity [*Schultz et al.*, 1996], we can nevertheless infer that vertical velocities at a given site must be greater than zero (positive upward) if exit fluid temperatures are greater than those measured in the overlying water column. Conversely, because near-surface thermal gradients across the mound are everywhere positive downward [*Becker et al.*, 1996], vertical velocities must be small or negative (i.e., flow into the seafloor) during periods when exit fluid temperatures are the same as those in the overlying water column. These simple constraints allow us to use the temperature records to make first-order distinctions between periods of active hydrothermal discharge and periods of no flow or recharge for individual sites during the deployment. This strict distinction is not possible for the high-temperature records, which clipped low at ~150°C, and thus cannot formally be used to discern periods of no flow.

[16] The temperature records can be characterized as alternating between periods of flow, and no flow, at varying intervals. The transition between flow states can occur as either an abrupt perturbation or a more gradual rise, with abrupt perturbations being more common, overall. Abrupt temperature perturbations, both positive and negative, are also ubiquitous during flow episodes, and the space-time pattern of temperature perturbations on the mound has a strong random quality. Sometimes a set of probes will respond to a common event, but other times they will not. Each temperature record has a unique perturbation structure that is difficult to relate in a deterministic way with that of any other, even though there are some obvious similarities.

[17] To illustrate some of the episodic characteristics of the data, we consider the 16-day interval from days 244–260 (4–20 September 2003) on a subset of the temperature records (Figure 7). Just before day 246 there was an apparent event (labeled 1) that triggered temperature perturbations and/or flow episodes on several low-temperature probes (L4, L5, L11), but each responded in a different way. Temperatures at probe L5 (located in ODP 6 depression on the west side of the upper terrace), which was 5 days into a low-amplitude (~2°C above background) episode, rose 15°C over a period of 7 hours. Fluid temperatures then briefly spiked up to 46°C for about 40 min before stabilizing at ~15°C for the next four days. Probes L9 and L12, both located within 10 m of probe L5 in the ODP 6 depression, did not respond to this event.

[18] Four hours and 48 min after temperatures began to rise at probe L5, temperatures at probe L4, located 30 m to the west at the base of the central black smoker complex, rose by 18°C over a period of 40 min. Prior to this, temperatures at probe L4 had been stable at ~7°C for the previous day, but overall temperatures at this site were highly variable and frequently clipped at the threshold value of 51.3°C for the first 80 days of the experiment (see Figure 5). After the fast initial rise, temperatures at probe L4 decayed steadily to ~2°C above background over the next 17 hours, before another abrupt perturbation (of 45°C, event 2 in Figure 7) continues the pattern of high-variability characterizing the period from July to September (2003) at this site.

[19] At approximately the same time that temperatures shot up rapidly at probe L4, temperatures at probe L11, located ~40 m south of probe L4 near the ODP reentry

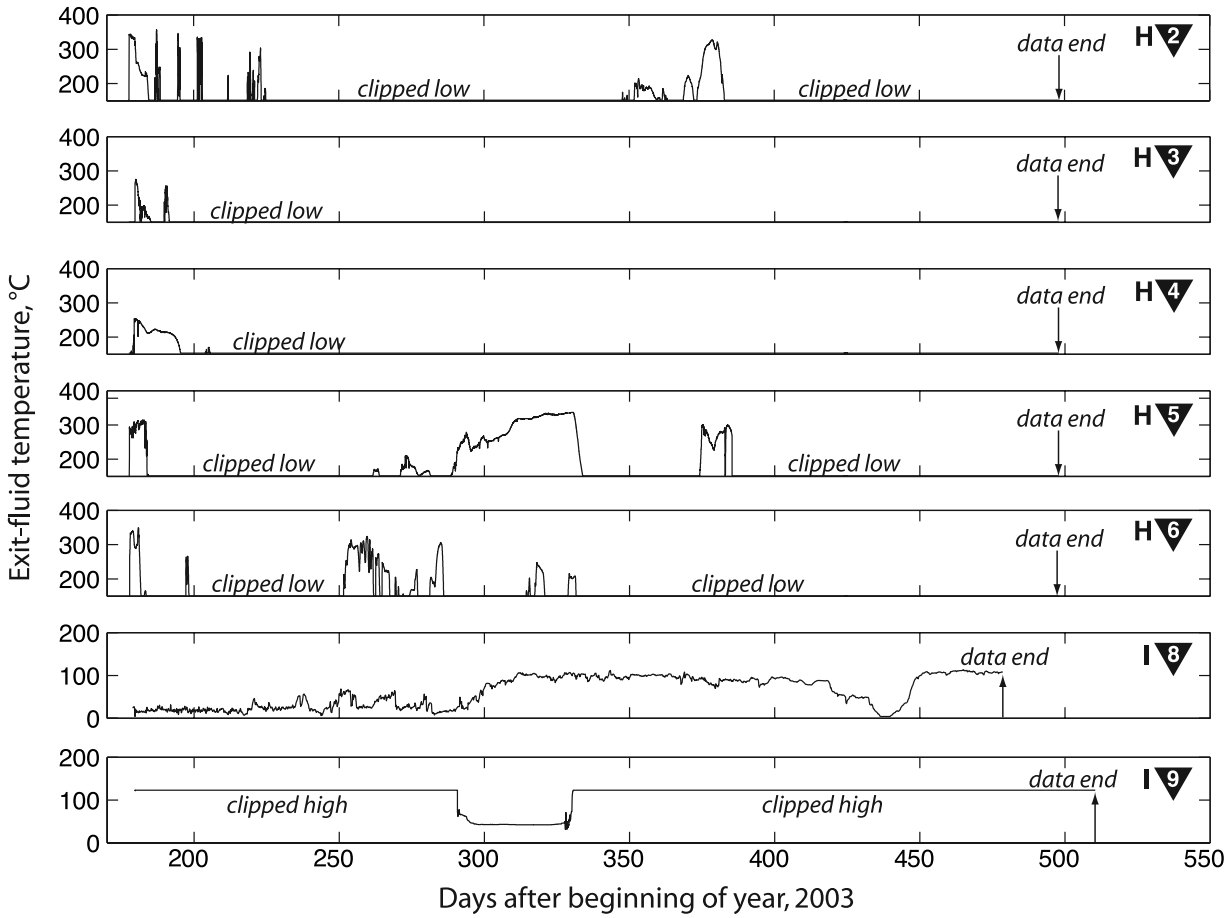

Figure 4. High-temperature (H2, H3, H4, H5, H6) and intermediate-temperature (I8, I9) exit fluid temperature records. Time axis is shown in days from the beginning of 2003. Note that all of the high-temperature probes clipped low at ~150°C for extended periods of time and that intermediate-temperature probe I9 clipped high at ~120°C for most of the deployment.

cones, began to pulse at semidiurnal periods (see section 4 for a description of tidal "chugging"). Temperatures at probe L11 had been at background water column levels for the previous two days, but this event marked the onset of a flow episode that would last the next 150 days, with average and maximum values of 9.2°C and 31°C above background, respectively. We thus observe that the event that occurred during day 245 (event 1 in Figure 7), affected temperatures at probes L5, L4, and L11, each in a different way, but did not affect any of the other probes, even though probes L9, L12, H6, and H5 were all located within 10 m an affected probe.

[20] Although probe L9 did not covary with probe L4 during the first event, it does covary during the next event (event 2 in Figure 7), while, interestingly, probe L5 does not. Temperatures at probe L9 begin to rise two and a half hours before the 45°C perturbation at probe L4, with an oscillation at ~54 min period. Temperatures at probe L9 peak at 16°C above background 5 h 17 m into the episode, which lasted 87 days with an average value of 3°C above background. Probe L9 also appears to covary with probe L4 during event 3, but this time an inverse correlation is observed as temperatures drop ~10°C in 16 min (i.e., 2 samples) a little more than three hours before the rapid rise at probe L4. Events 4 and 6, which are also associated with large temperature perturbations at probe L4, did not significantly affect probe L9, nor any of the other probes.

Figure 5. Low-temperature exit fluid temperature records displayed clockwise around the mound starting with probe L12 in the ODP 6 depression. Two records are shown for each probe, corresponding to the pairs deployed at the end of each plastic wand. (left) Time series data and (right) data histograms. The *y* axis of the histograms represents normalized frequency, which is the number of observations in each data bin divided by the total number of observations (data are binned in digitization bins of the data loggers). Many of the records contained large fractions of measurements in the first few data bins corresponding to background water column temperature levels (~2.7°C), and in such cases a small *y* axis interval of 0–0.1 is retained to bring out the details of the histogram shape, but the fraction of observations in the background temperature bins is explicitly listed (e.g., the two probes at site L12 returned background temperature measurements 45% and 56% of the time, respectively.

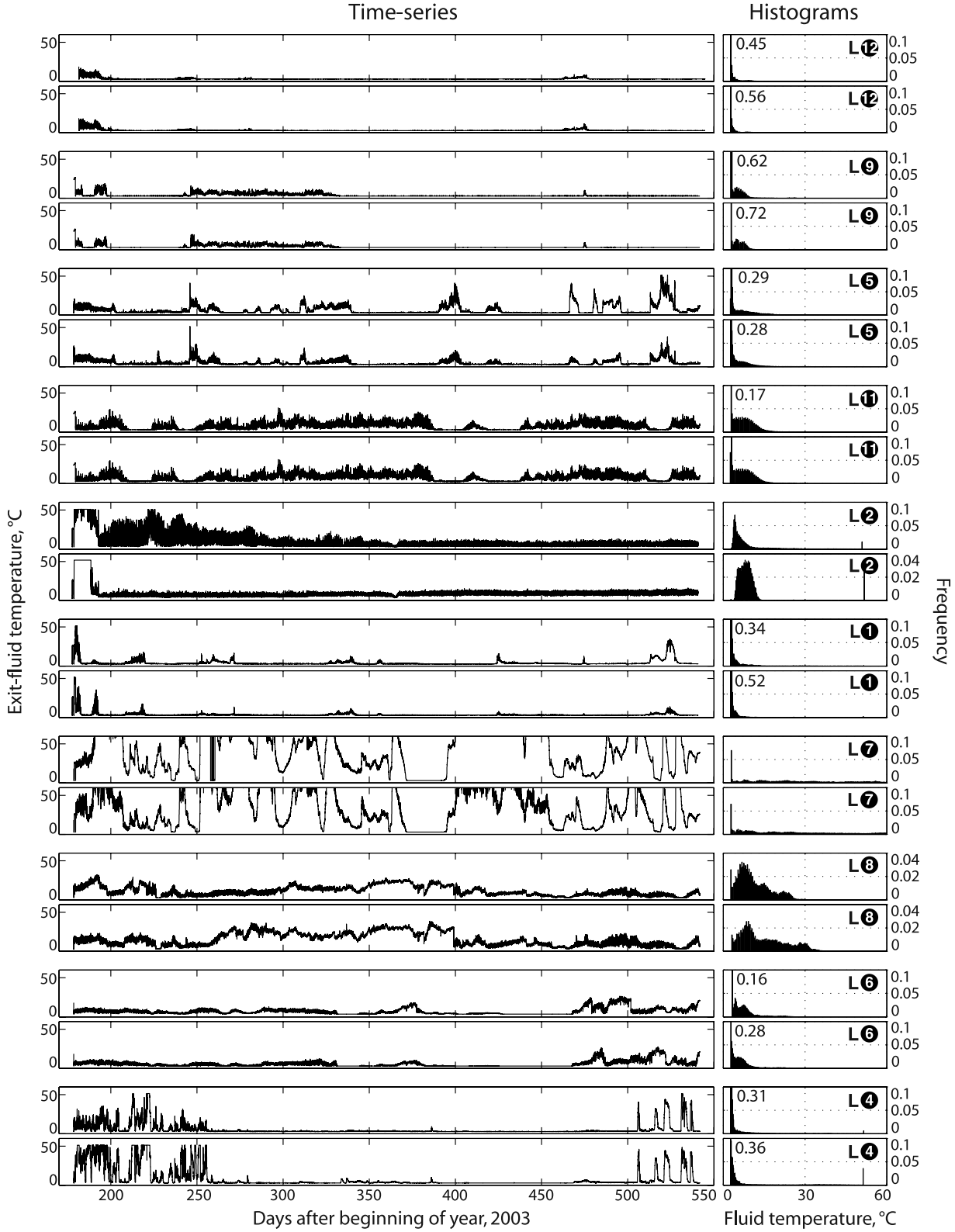
Time-series
Histograms
0.45
0.56
0.62
0.72
0.29
0.28
0.17
0.34
0.52
0.16
0.31
0.36
Exit-fluid temperature, °C
Frequency
Days after beginning of year, 2003
Fluid temperature, °C

Figure 5

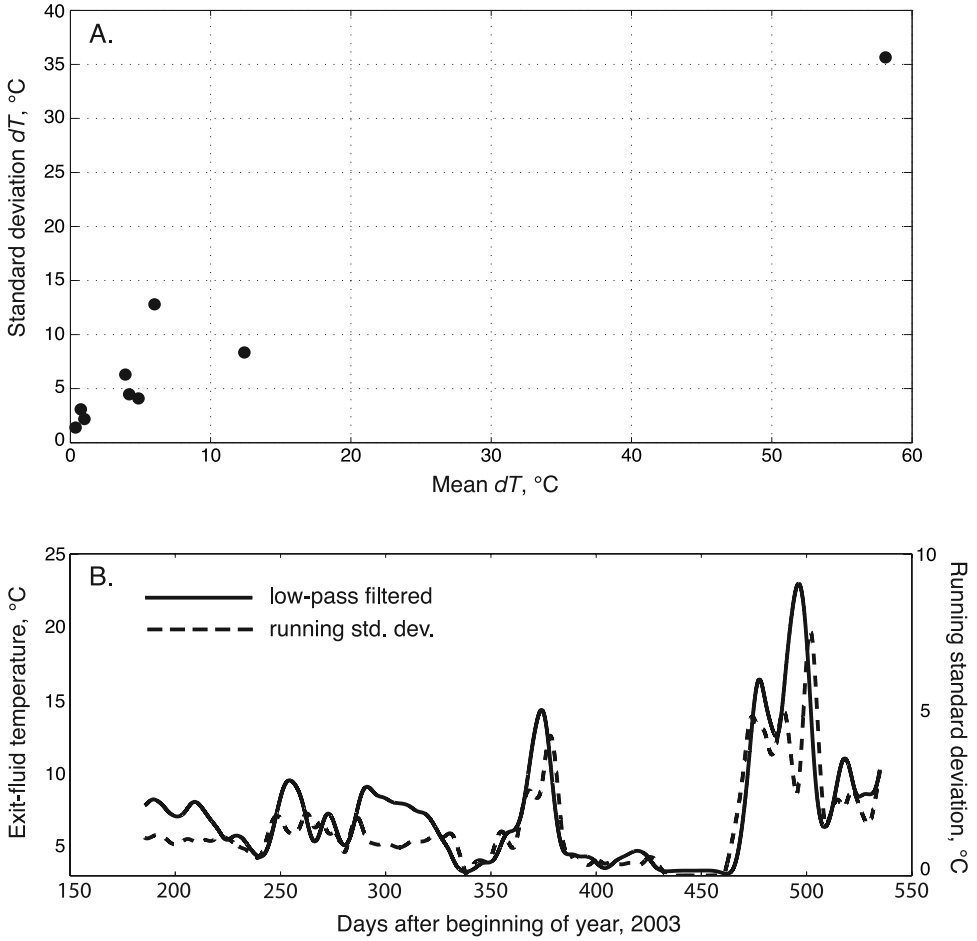

Figure 6. Relationship between data mean and variance. (a) Overall relationship between mean values and standard deviations from Table 1 for the unclipped temperature records (low-temperature probes L1, L4, L5, L6, L8, L9, L11, L12, and intermediate-temperature probe I8). (b) Instantaneous relationship between time-averaged mean and variance. Solid line is the low-pass-filtered (4 pole Butterworth, 12-day corner period) temperature time series data for diffuse flow probe L6. Dashed line is the "running" standard deviation, which is calculated by finding the standard deviation of the temperature measurements in a 12-day window centered about each time step. The data in each 12-day interval are weighted by a Gaussian window for the standard deviation calculation.

[21] We do not know if high-temperature probe H6, located in the ODP 6 depression with probes L5, L9, and L12, responded to events one through four (for clipping reasons), but we do observe an apparent correlation with a perturbation (event 5 in Figure 7) on probe L7, which was located ~50 m away on the opposite side of the upper terrace. Temperatures at H6 were at or below the clipping threshold of 150.1°C for 53 days prior to event 5, but then began to rise to a maximum value of 254°C over the next 2.5 days during the course of a ~34 day episode containing strong diurnal oscillations. Temperatures at probe L7, which had been hovering at or just above background levels for two days, begin to rise three days and 17 hours after the perturbation from event five is observed at probe H6, reaching the clipping threshold of 70.6°C about 12 hours later. The ensuing episode at probe L7 lasted 120 days and averaged >43°C (high-end clipping precludes precise estimate of mean). Event 5 did not appear to affect temperatures at any probes other than H6 and L7.

[22] We can examine the nature of episodic perturbations across the mound as a whole by considering the running-average time series of all the diffuse flow records (Figure 8). Although the timing and number of episodic perturbations is unique for each temperature record, many of the perturbations are well enough correlated across the mound to remain evident in the running average. We also see that the mean value of the running-average time series is stable at ~10°C on the timescale of the experiment duration.

4. Harmonic Variability and Tidal Periods

[23] All of the temperature records exhibit harmonic oscillations over a range of periods, with the strongest effects observed in the diffuse flow data at diurnal and semidiurnal tidal cycles. Stochastic power spectra estimates from the unclipped diffuse flow records are shown in Figure 9. Overall, the spectra are red over periods from 100 days to 3 hours with decay at a rate of ~17 dB/decade, with spectral peaks being most pronounced at 1 and 2 cpd

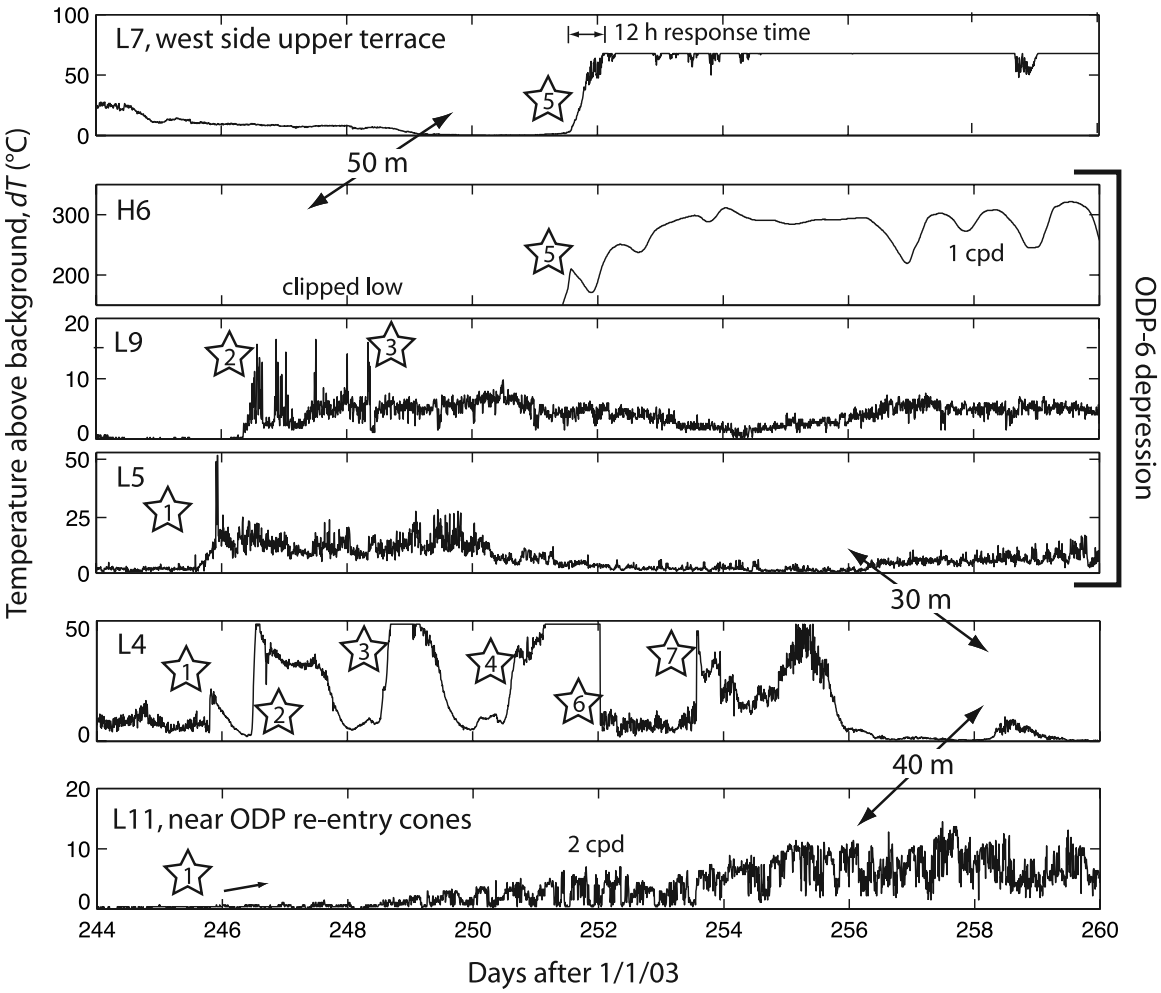

Figure 7. Case study of episodic perturbations from days 244 to 260 (4–20 September 2003) on probes L7, H6, L9, L5, L4, and L11. Flow events are shown as sequentially labeled starts for those probes that exhibit an apparent response. See text in section 3 for description.

periods. The diurnal (1 cpd) and semidiurnal (2 cpd) peaks correspond to lunar (i.e., O1 and M2), rather than solar, frequencies [e.g., *Schwiderski*, 1980]. Spectral peaks at 3 and 4 cpd are also evident in some records, which may correspond to the resonant modes O1 + M2 (M3) and M2 + M2 (M4), respectively [e.g., *Parker*, 1991]. Such resonant modes are observed in shallow, semienclosed features such as estuaries [e.g., *Blanton et al.*, 2002; *Friedrichs and Aubrey*, 1988], while in this case they may result from topographically trapped waves in the axial valley. These and other tidal forcing periods and resonances were also observed in pressure and temperature records from a deep-sea tide gauge deployed ~400 m northwest of the mound (in a region of no hydrothermal discharge) [*Reves-Sohn et al.*, 2006].

[24] We observed a special kind of behavior at the diffuse flow sites during certain times when exit fluid temperatures were hovering near background water column levels. During these periods of time fluid temperatures pulse at

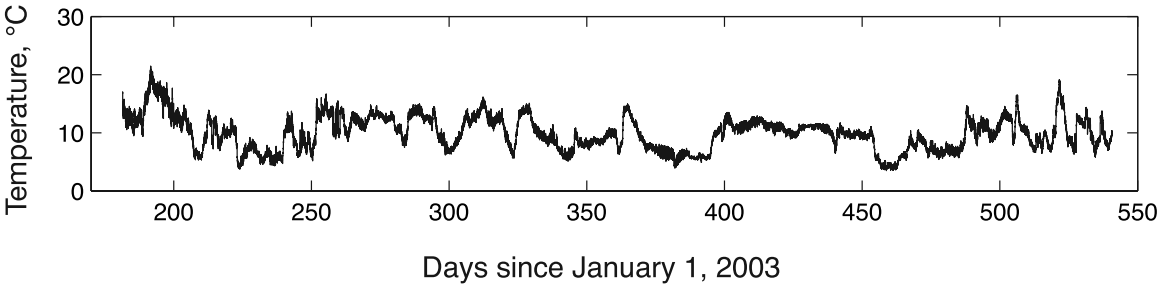

Figure 8. Running-average time series of diffuse flow probes L1, L4, L5, L6, L7, L8, L9, L11, and L12. The mean value of exit fluid temperature is calculated for these probes at each common time step. The overall mean value of the running-average time series is 9.9°C.

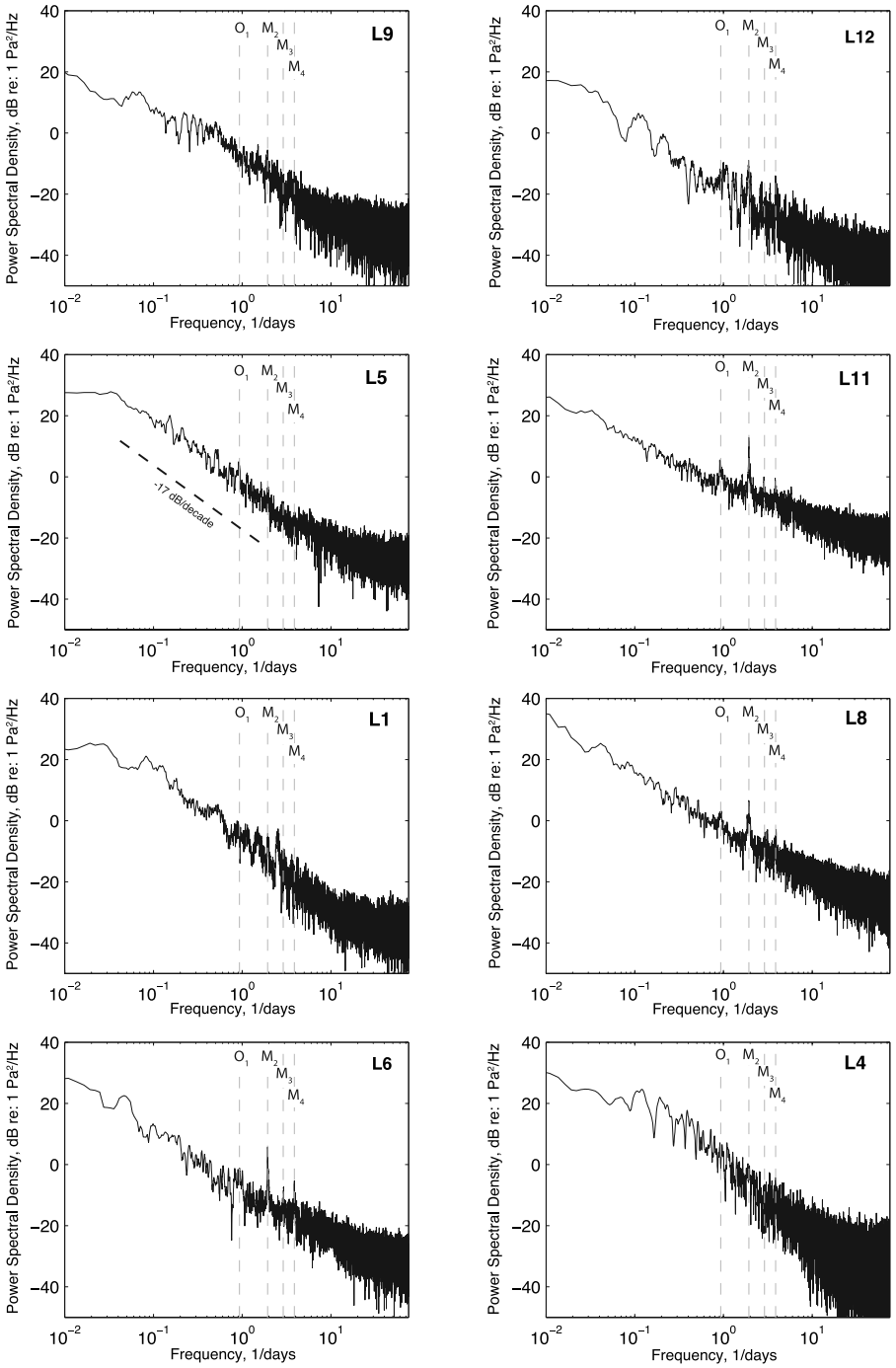

Figure 9. Stochastic power spectra estimates for diffuse flow probes L1, L4, L5, L6, L8, L9, L11, and L12 (same probes used to generate running-average time series). Multitaper methods with a time-bandwidth product NW = 3 were used to estimate spectral levels using the entire time series for each site. The lunar tidal periods O1, M2, M3, and M4 are shown as dashed gray vertical lines at the appropriate frequencies. Note that spectral peaks are evident at periods other than tidal cycles, particularly at low frequencies.

tidal periods with an amplitude of 0.1–0.6°C, and with the low-amplitude side of the harmonic oscillation being truncated at the background temperature value (Figure 10). This phenomenon suggests that the local flow regime at the monitoring site during these times is delicately balanced about an equilibrium, with flow out of the seabed during one half of the tidal cycle and flow into the seabed during the other half of the cycle. If the water column is locally isothermal, and there is a thermal gradient (positive downward) below the seafloor interface [e.g., *Becker et al.*, 1996], then flow reversals generated by tidal pressure cycles will generate the truncated temperature signals observed in

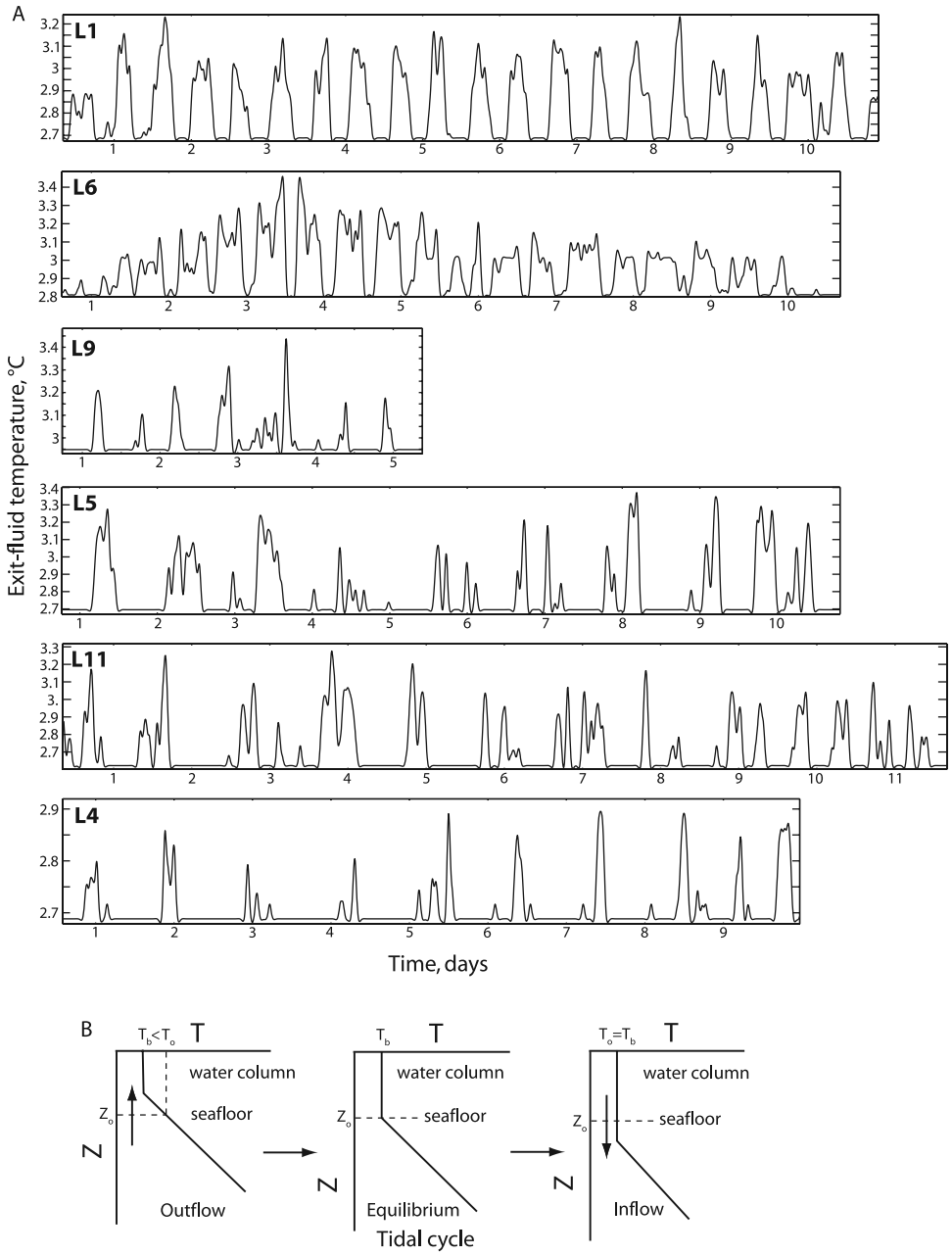

Figure 10. Tidal pulsing cycle. (a) Examples of tidal pulsing when exit fluid temperatures are hovering near background levels for diffuse flow probes L1, L6, L9, L5, L11, and L4. L1, L6, and L9 are chugging at 2 cpd (semidiurnal period). L4 is pulsing at 1 cpd (diurnal period), and L5 and L11 are pulsing at a mixture of both semidiurnal and diurnal periods. All of the records are low-pass filtered with a 2 hour corner frequency. (b) Conceptual flow model for pulsing. Pulsing can occur when the flow regime at a sensor is delicately balanced about an equilibrium point of no net flow (i.e., the sensor is at a flow node between regions of discharge and recharge). The equilibrium thermal gradient is isothermal at background water column levels above the seafloor and positive downward within the hydrothermal deposit. Tidal pressure perturbations modulate this thermal gradient about the equilibrium point to generate the observed temperature signal. Outflow (i.e., discharge) during low pressure (low tide) displaces the equilibrium gradient upward thereby elevating fluid temperatures several tenths of a degree centigrade above background (i.e., $T_{observed} > T_{background}$). Inflow (i.e., recharge) during high pressure (high tide) displaces the equilibrium gradient downward thereby reducing fluid temperatures to background water column levels (i.e., $T_{observed} = T_{background}$). This results in a temperature record that pulses positive at tidal forcing periods.

the diffuse flow records (Figure 10). This tidal pulsing phenomenon occurs at both diurnal and semidiurnal periods, and is consistent the flow reversals predicted by poroelastic models of tidal loading for regions of very small net fluxes (i.e., no net flow) [*Crone and Wilcock*, 2005], as described in section 5.2.

5. Discussion

[25] The exit fluid temperature records and analytical results described above provide new insight into the patterns of space-time flow variability within the active TAG hydrothermal mound on timescales from ~10 min up to the yearlong period of observation. Here I interpret the results and make inferences regarding the characteristics of subsurface flow. My interpretations are primarily based on analyses of the diffuse flow records because of the clipping issues that hinder quantitative analysis of the high-temperature records.

[26] One of the most basic observations is the correlation between the data mean and variance (Figure 6). This relationship holds both in terms of the long-run statistics (Figure 6a) and at the instantaneous level (Figure 6b). In other words, along with the fact that there is a correlation between the year-averaged mean and variance of the individual temperature records, we also find that the higher the instantaneous discharge temperature at a given point in time, the higher the short-term variability. This proportionality between the vigor and variability of flow is an important constraint for any circulation model of the active TAG mound. For stochastic flow modeling this suggests the use of Gamma density functions, as described by *Sohn* [2007].

5.1. Flow Episodes and Reorganization of Diffuse Flow Patterns

[27] Both the black smoker and diffuse flow temperature records exhibit a high degree of episodic variability, with complex spatial correlations across the mound. Episodic, or aperiodic, temperature variations have previously been observed in diffuse flow records from the active TAG mound over a ~7 day period of observation by *Kinoshita et al.* [1996] and *Schultz et al.* [1996], and this work expands on those results by observing the nature of repeated episodic variations at multiple monitoring sites across the mound over a yearlong period of observation. All of the low-temperature records acquired from sites of diffuse discharge alternate between periods when temperatures are equal to background water column values and periods when temperatures are elevated by as much as 60+°C. As described previously, this allows us to make a first-order distinction between periods of active discharge when vertical fluid velocities are positive upward (i.e., periods when fluid temperatures are above background) and periods of no discharge when vertical velocities are near zero or perhaps positive downward (i.e., recharge).

[28] The relative proportion of time spent in periods of discharge versus no discharge is variable across the mound (see Table 1). For example, probes L5, L9, and L12, which were all deployed within ~10 m of each other in the ODP 6 depression, were discharging hydrothermal fluid (i.e., had positive temperature anomalies) 56%, 27%, and 14% of the time, respectively. By contrast, probes L6 and L8, located ~25 m apart on the northwest shoulder of the black smoker complex, were discharging hot fluid 83% and 97% of the time, respectively. Overall, diffuse discharge was stronger and more consistent at sites on the west side of the mound. On average, the diffuse flow sites monitored during the experiment discharged hot fluid 61% of the time, and had fluid temperatures equal to background levels 39% of the time. If we account for the sampling bias introduced by only deploying probes in sites discharging hot fluid at the beginning of the experiment by discarding the first two months of data, we find that the diffuse flow sites monitored during the experiment were actively discharging fluids 55% of the time. I thus find that diffuse flow sites at the TAG mound were about equally likely, on average, to be in a state of discharge or no discharge/recharge at any given time during the experiment, with a bias toward more discharge on the west side of the mound and more recharge on the east side.

[29] These results demonstrate that the locations of diffuse discharge were continually changing, which means that the shallow subsurface flow patterns were also continually changing. At individual sites the characteristic thermal response time to these perturbations is on the order of a few days, and from the running-average time series for the diffuse flow records, which is stable at ~10°C over the long-term (Figure 8), we find that the perturbations did not affect the overall vigor of diffuse discharge at timescales longer than about a month. All of this evidence taken together suggests that the episodic temperature perturbations primarily represent reorganizations, rather than amplitude modulations, of the diffuse flow field. The temperature of diffuse flow in hydrothermal systems is closely related to near-surface permeability [*Pascoe and Cann*, 1995], and the simplest way to reorganize flow and generate episodic perturbations of the kind exhibited in our temperature records is to perturb the permeability structure. The sulfide structure is intrinsically unstable owing to gravitational stresses and anhydrite dissolution, and mechanical perturbations from nearby earthquakes, or intrinsic processes such as hydrofracture or gravitational collapse, provide plausible mechanisms for episodically perturbing the near-surface permeability field and reorganizing diffuse flow within the hydrothermal deposit. These considerations lead to the interpretation that diffuse flow patterns are continually perturbed and reorganized in the subsurface by changes to the permeability structure of the hydrothermal deposit. A stochastic model for these episodic variations is provided in the companion paper [*Sohn*, 2007].

5.2. Response to Tidal Forcing

[30] Harmonic oscillations at a variety of periods were observed for both the black smoker and diffuse flow records (Figure 9). The strongest signals were observed for lunar (as opposed to solar) modes O1 and M2 on the diffuse flow records, and harmonics at M3 and M4 periods are evident at some sites. These results are consistent with analyses of previously acquired, shorter duration (~7 day long) diffuse flow records from the active TAG mound, which also found strong variability at tidal periods, with M2 being dominant [*Kinoshita et al.*, 1996; *Schultz et al.*, 1996].

[31] We can gain insight into the nature of tidal forcing at the TAG field by considering the tidal pulsing observed in

the diffuse flow records and reported here for the first time. During certain time periods when exit fluid temperatures are at, or just barely above, background water column levels, temperatures at diffuse flow sites pulse at tidal periods (both diurnal and semidiurnal) with a low-amplitude (0.1–0.6°C) sinusoidal pattern truncated on the low end at the background level of ~2.7°C (Figure 10). If we assume that the local temperature gradient at these sites is positive downward into the seafloor but isothermal in the water column, then these temperature pulses are consistent with flow reversals. This phenomenon presumably occurs when a probe is located at a flow node between domains of discharge and recharge, such that the net fluid flux is near zero. Exit fluid temperatures are equal to background water column levels when fluids are being drawn into the seafloor, and are then elevated above background during periods of discharge (Figure 10b). These kinds of flow reversals at tidal periods in regions of low net flux are predicted by poroelastic models of hydrothermal flow [*Crone and Wilcock*, 2005].

[32] If we apply this result to the data in a general way, and assume that diffuse recharge was occurring whenever exit fluid temperatures were at background water column levels, we find that diffuse recharge was occurring at the monitoring sites roughly half the time (45%) during the experiment, with relatively more recharge occurring on the east side of the mound (e.g., probe sites 5, 9, and 12) compared to the west (e.g., probe sites 6 and 8) based on the flow statistics. This result implies that both discharge and recharge for diffuse flow are accommodated on the same set of fractures within the shallow TAG mound, and, when the nature of episodic variability from section 5.1, is considered, we can infer that the spatial patterns of discharge and recharge are continually reorganized in an apparently random way by perturbations to the shallow permeability structure. Geochemical studies have shown that diffuse flow at TAG represents a secondary recirculation system [e.g., *Tivey et al.*, 1995] that is coupled to primary discharge via conduction across the primary conduit walls [e.g., *Sleep*, 1991], such that permeability changes to either the mineralized sheath of the primary conduit walls or the diffuse flow cracks, themselves, could explain the observed modes of variability.

[33] Two models have been put forward to explain the observation of tidal harmonics in exit fluid temperature records from deep-sea vent fields. One model invokes effects from tidal currents flowing horizontally over discharge features [*Tivey et al.*, 2002], while the other invokes poroelastic effects from tidal pressure perturbations in the shallow subsurface flow environment [*Crone and Wilcock*, 2005; *Jupp and Schultz*, 2004]. The truncated sinusoidal temperature signals observed during tidal pulsing at TAG are consistent with flow reversals from poroelastic effects of tidal loading [*Crone and Wilcock*, 2005], but are inconsistent with forcing from currents, which cannot explain the truncated lower end of the signal without invoking physically implausible water column structure.

[34] In principle, the phase lag between tidal pressure and the exit fluid temperature signal can be used to deduce hydrologic properties of the near-surface flow field [*Crone and Wilcock*, 2005; *Jupp and Schultz*, 2004]. We do in fact have tidal pressure records during the first half of our monitoring experiment [*Reves-Sohn et al.*, 2006], but estimation of the cross-spectral phase angle is complicated by timing uncertainties for the temperature probes, which, for logistical reasons, were not recovered before their clock batteries died. It may be possible to correct for clock drift by synching spectral peaks in the temperature probe and tide gauge records, but this is beyond the scope of the present analysis. We can see that the amplitude of tidal variability during flow reversals (0.1–0.6°C) is somewhat larger than that predicted for a homogeneous medium [e.g., *Crone and Wilcock*, 2005], which seems to require a heterogeneous permeability structure within the deposit, which is not at all surprising.

[35] Although the diffuse temperature records provide good evidence for poroelastic effects from tidal loading, we nevertheless cannot discount tidal currents as a mechanism for modulating exit fluid temperatures. Near-bottom currents at TAG exhibit both diurnal and semidiurnal periodicity [*Wichers et al.*, 2005], and although we did not observe bottom currents during the temperature monitoring experiment, tide gauge pressure and temperature records (simultaneously observed 400 m northwest of the mound) provide evidence for complex modes of barotropic and baroclinic tidal dynamics in the water column above the hydrothermal field [*Reves-Sohn et al.*, 2006].

5.3. Synoptic Flow Model

[36] Here I interpret the exit fluid temperature results within the context of the large-scale convection system of the TAG field. Microearthquake and seismic refraction results have shown that hydrothermal fluids must penetrate to depths of 7+ km below the seafloor to extract heat to drive high-temperature convection at the TAG hydrothermal field [*Canales et al.*, 2005; *deMartin et al.*, 2005]. Circulation at midcrustal to lower crustal depths is likely restricted to the long-lived, dome-shaped, extensional fault surface that extends to mantle depths on the east side of the axial valley [*deMartin et al.*, 2007]. At shallower depths (less than ~1 km) flow is not restricted to the fault surface, and the position of the high-temperature deposits on the fault hanging wall demonstrates that most of the hot fluids depart the fault surface within the volcanic section [e.g., *Humphris and Cann*, 2000].

[37] Repeat observations of the chronic water column plume above the TAG field [cf. *Rona and Speer*, 1989; *Wichers et al.*, 2005] and repeat dive observations of the active TAG mound [e.g., *Edmond et al.*, 1995; *Rona et al.*, 1986; *Temple et al.*, 1979; *Thompson et al.*, 1988, 1985] indicate that the vigor of overall discharge has changed very little on the decadal scale. This suggests that flow within the primary conduit that feeds the active TAG mound is stable on these same timescales, such that ~360°C fluids are continuously discharged with a thermal power that has been estimated at somewhere between 0.55 and 3.0 GW [cf. *Goto et al.*, 2003; *Rona and Speer*, 1989; *Wichers et al.*, 2005]. We were not able to deploy any temperature probes within this primary discharge field, unfortunately, because of our inability to access the central black smoker chimney.

[38] At shallower depths near the seafloor, the robust primary flow system fuels a secondary circulation system [*Tivey et al.*, 1995] that draws ambient seawater into the deposit along flow conduits generated by fissuring and faulting in the hanging wall of the extensional fault and

by gravitational stresses and dissolution within the deposit itself. The secondary circulation system may be composed of multiple convection cells, possibly organized in a radial configuration along the ring crack on the perimeter of the upper terrace. The flow patterns within the secondary convection system are continually perturbed by an as of yet poorly understood combination of extrinsic and intrinsic mechanisms, and these perturbations rapidly reorganize the patterns of discharge and recharge on timescales of order $\sim$1 day. Flow within the secondary circulations systems is also modulated by the pressure and velocity field of the overlying water column at a variety of forcing periods, with diurnal and semidiurnal cycles being dominant.

[39] Overall, exit fluid temperatures measured on the active TAG mound exhibit considerably more variability than records acquired over similar time intervals from vent fields on the EPR [e.g., *Scheirer et al.*, 2006]. This increased variability is likely related to fundamental hydrogeological differences between massive sulfide deposits hosted in extensional terrains on slow spreading mid-ocean ridges and ephemeral discharge features on magmatically robust fast spreading mid-ocean ridges [*Wilcock and Delaney*, 1996]. The hanging wall hosting the TAG hydrothermal field is also continually perturbed by seismic events on the long-lived extensional fault [*deMartin et al.*, 2007], which may also be a source of flow variability. Statistical assessment of the correlation between seismicity catalogues compiled from a 9-month-long microearthquake survey of the TAG region and the exit fluid temperature records presented here is an important topic of future research.

[40] The high levels of exit fluid temperature variability we observed at the TAG mound caused problems for the temperature probes, which did not have sufficient bandwidth to capture the full range of temperature variations at many monitoring sites. These clipping issues effectively precluded the use of high-temperature records in our stochastic analysis, but they can be easily solved by employing higher bandwidth data loggers for future experiments. The DSPL and MiniLogger probes utilize 8-bit data loggers, which should be upgraded to 12 or 16 bits for future monitoring experiments at slow spreading vent fields.

[41] **Acknowledgments.** This work owes a debt of gratitude to many more individuals than can be named here. First and foremost, however, I would like to thank my co-PIs on the Seismicity and Fluid Flow of TAG experiment, Susan Humphris and J. Pablo Canales, for their sustained efforts over the past 5 years to help conceive and carry out the field program and to analyze and interpret the resulting data sets. Dan Fornari's efforts to develop, fabricate, and test the temperature probes were also crucial to this effort, as was the dedicated service of the officers and crews of the R/Vs *Atlantis* and *Knorr* and the engineers and technicians in the Deep Submergence Lab at WHOI, who supported our *Alvin* and *Jason* 2 dive programs at sea. Kevin Speer and William Wilcock provided constructive reviews that have substantially improved the manuscript. This work was supported by the National Science Foundation (OCE-0137329).

References

Baker, E. T., C. G. Fox, and J. P. Cowen (1999), In-situ observations of the onset of hydrothermal discharge during the 1998 submarine eruption of Axial volcano, Juan de Fuca Ridge, *Geophys. Res. Lett.*, *26*, 3445–3448.

Becker, K., R. P. Von Herzen, J. Kirklin, R. L. Evans, D. Kadko, M. Kinoshita, O. Matsubayashi, R. Mills, A. Schultz, and P. A. Rona (1996), Conductive heat flow at the TAG active hydrothermal mound: Results from 1993–1995 submersible surveys, *Geophys. Res. Lett.*, *23*, 3463–3466.

Blanton, J. O., G. Lin, and S. A. Elston (2002), Tidal current asymmetry in shallow estuaries and tidal creeks, *Continental Shelf Res.*, *22*, 1731–1743.

Campbell, A. C., et al. (1988), Chemistry of hot springs on the Mid-Atlantic Ridge, *Nature*, *335*, 514–519.

Canales, J. P., R. Reves-Sohn, and S. E. Humphris (2005), Tectonism and long-lived hydrothermal systems: The TAG segment, Mid-Atlantic Ridge 26°N, *Eos Trans. AGU*, *86*, Fall Meet. Suppl., Abstract OS33A-1467.

Cherkaoui, A. S. M., W. S. D. Wilcock, and E. T. Baker (1997), Thermal fluxes associated with the 1993 diking event on the CoAxial Segment, Juan de Fuca Ridge: A model for the convective cooling of a dike, *J. Geophys. Res.*, *102*, 24,887–824,902.

Chevaldonne, P., D. Desbruyeres, and M. L. Haitre (1991), Time-series of temperature from three deep-sea hydrothermal vent sites, *Deep Sea Res., Part A*, *38*, 1417–1430.

Crone, T. J., and W. S. D. Wilcock (2005), Modeling the effects of tidal loading on mid-ocean ridge hydrothermal systems, *Geochem. Geophys. Geosyst.*, *6*, Q07001, doi:10.1029/2004GC000905.

Davis, E., K. Becker, R. Dziak, J. Cassidy, K. Wang, and M. Lilley (2004), Hydrological response to a seafloor spreading episode on the Juan de Fuca ridge, *Nature*, *430*, 335–338.

deMartin, B., R. Reves-Sohn, J. P. Canales, and S. E. Humphris (2005), Microearthquake survey of the TAG segment, Mid-Atlantic Ridge (26°N): The early stages of deformation on a detachment fault revealed, *Eos Trans. AGU*, *86*(52), Fall Meet. Suppl., Abstract T33G-03.

deMartin, B. J., R. A. Sohn, J. P. Canales, and S. E. Humphris (2007), Kinematics and geometry of active detachment faulting beneath the TAG hydrothermal field on the Mid-Atlantic Ridge, *Geology*, in press.

Edmond, J. M., A. C. Campbell, M. R. Palmer, G. P. Klinkhammer, C. R. German, H. N. Edmonds, H. Elderfield, G. Thompson, and P. A. Rona (1995), Time series studies of vent fluids from the TAG and MARK sites (1986, 1990) Mid-Atlantic Ridge: A new solution chemistry model and mechanism for Cu/Zn zonation in massive sulfide orebodies, in *Hydrothermal Vents and Processes*, edited by L. M. Parson et al., *Geol. Soc. Spec. Publ.*, *85*, 77–86.

Fornari, D., C. L. Van Dover, T. Shank, R. Lutz, and M. Olsson (1994), A versatile, low-cost temperature sensing device for time-series measurements at deep sea hydrothermal vents, *BRIDGE Newsl.*, *6*, 37–40.

Fornari, D. J., F. Voegeli, and M. Olsson (1996), Improved low-cost, time-lapse temperature loggers for deep ocean and sea floor observatory monitoring, *RIDGE Events*, *7*, 13–16.

Friedrichs, C. T., and D. G. Aubrey (1988), Non-linear tidal distortion in shallow well-mixed estuaries: A synthesis, *Estuarine Coastal Shelf Sci.*, *27*, 521–545.

Fujioka, K., K. Kobayashi, K. Kato, M. Aoki, K. Mitsuzawa, M. Kinoshita, and A. Nishizawa (1997), Tide-related variability of TAG hydrothermal activity observed by deep-sea monitoring system and OBSH, *Earth Planet. Sci. Lett.*, *153*, 239–250.

Gebruk, A. V., S. V. Galkin, A. L. Vereschaka, L. I. Moskalev, and A. J. Southward (1997), Ecology and biogeography of the hydrothermal vent fauna of the Mid-Atlantic Ridge, *Adv. Mar. Biol.*, *32*, 93–144.

Goto, S., M. Kinoshita, A. Schultz, and R. P. Von Herzen (2003), Estimate of heat flux and its temporal variation at the TAG hydrothermal mound, Mid-Atlantic Ridge 26°N, *J. Geophys. Res.*, *108*(B9), 2434, doi:10.1029/2001JB000703.

Huang, P. Y., and S. C. Solomon (1988), Centroid depths of mid-ocean ridge earthquakes: Dependence on spreading rate, *J. Geophys. Res.*, *93*, 13,445–13,477.

Humphris, S. E., and J. R. Cann (2000), Constraints on the energy and chemical balances of the modern TAG and ancient Cyprus seafloor sulfide deposits, *J. Geophys. Res.*, *105*, 28,477–28,488.

Johnson, H. P., M. Hutnak, R. P. Dziak, C. G. Fox, I. Urcuyo, J. P. Cowen, J. Nabelek, and C. Fisher (2000), Earthquake-induced changes in a hydrothermal system on the Juan de Fuca mid-ocean ridge, *Nature*, *407*, 174–177.

Jupp, T. E., and A. Schultz (2004), A poroelastic model for the tidal modulation of seafloor hydrothermal systems, *J. Geophys. Res.*, *109*, B03105, doi:10.1029/2003JB002583.

Kinoshita, M., O. Matsubayashi, and R. P. Von Herzen (1996), Sub-bottom temperature anomalies detected by long-term temperature monitoring at the TAG hydrothermal mound, *Geophys. Res. Lett.*, *23*, 3467–3470.

Lalou, C., J. L. Reyss, and E. Brichet (1998), Age of sub-bottom sulfide samples at the TAG active mound, *Proc. Ocean Drill. Program Sci. Results*, *158*, 111–117.

Parker, B. B. (1991), The relative importance of the various non-linear mechanisms in a wide range of tidal interactions (review), in *Tidal Hydrodynamics*, edited by B. B. Parker, pp. 237–268, John Wiley, New York.

Pascoe, A. R., and J. R. Cann (1995), Modelling diffuse hydrothermal flow in black smoker vent fields, in *Hydrothermal Vents and Processes*, edited by L. M. Parson et al., *Geol. Soc. Spec. Publ.*, *85*, 159–173.

Polzin, K. L., J. M. Toole, J. R. Ledwell, and R. W. Schmitt (1997), Spatial variability of turbulent mixing in the abyssal ocean, *Science*, *276*, 93–96.

Pruis, M. J., and H. P. Johnson (2004), Tapping into the sub-seafloor: Examining diffuse flow and temperature from an active seamount on the Juan de Fuca Ridge, *Earth Planet. Sci. Lett.*, *217*, 379–388.

Reves-Sohn, R., R. Thomson, and A. Rabinovich (2006), Tidal Dynamics in the Axial Valley of the Mid-Atlantic Ridge, *Eos Trans. AGU*, *87*(52), Fall Meet. Suppl., Abstract B31B-1101.

Roman, C. N., R. Reves-Sohn, H. Singh, and S. E. Humphris (2005), Self-consistent bathymetric mapping using sub-maps: Survey results from the TAG hydrothermal structure, *Eos Trans. AGU*, *86*(52), Fall Meet. Suppl., Abstract OS33A-1465.

Rona, P. A. (1980), TAG hydrothermal field: Mid-Atlantic Ridge crest at latitude 26°N, *J. Geol. Soc. London*, *137*, 385–402.

Rona, P. A., and K. G. Speer (1989), An Atlantic hydrothermal plume: Trans-Atlantic Geotraverse (TAG) area, Mid-Atlantic Ridge crest near 26°N, *J. Geophys. Res.*, *94*, 13,879–813,893.

Rona, P. A., G. Thompson, M. J. Mottl, J. A. Karson, W. J. Jenkins, D. Graham, M. Mallete, K. L. Von Damm, and J. M. Edmond (1984), Hydrothermal activity at the TAG hydrothermal field, Mid-Atlantic Ridge crest at 26°N, *J. Geophys. Res.*, *89*, 11,365–311,377.

Rona, P. A., G. P. Klinkhammer, T. A. Nelsen, J. H. Trefry, and H. Elderfield (1986), Black smokers, massive sulphides and vent biota at the Mid-Atlantic Ridge, *Nature*, *321*, 33–37.

Rona, P. A., M. D. Hannington, C. V. Raman, G. Thompson, M. K. Tivey, S. E. Humphris, C. Lalou, and S. Petersen (1993), Active and relict seafloor hydrothermal mineralization at the TAG hydrothermal field, Mid-Atlantic Ridge, *Econ. Geol.*, *18*, 1989–2017.

Rona, P. A., T. Ishihara, H. Chiba, H. Masuda, T. Oomori, M. C. Kleinrock, M. A. Tivey, M. Watanabe, and C. Lalou (1998), An active, low temperature hydrothermal mound and a large inactive sulfide mound found in the TAG hydrothermal field, Mid-Atlantic Ridge 26°N, 45°W, *Eos Trans. AGU*, *79*(45), Fall Meet. Suppl., F920.

Rubin, A. M. (1992), Dike-induced faulting and graben subsidence in volcanic rift zones, *J. Geophys. Res.*, *97*, 1839–1858.

Scheirer, D. S., T. M. Shank, and D. J. Fornari (2006), Temperature variations at diffuse and focused flow hydrothermal vent sites along the northern East Pacific Rise, *Geochem. Geophys. Geosyst.*, *7*, Q03002, doi:10.1029/2005GC001094.

Schultz, A., P. Dickson, and H. Elderfield (1996), Temporal variations in diffuse hydrothermal flow at TAG, *Geophys. Res. Lett.*, *23*, 3471–3474.

Schwiderski, E. W. (1980), On charting global ocean tides, *Rev. Geophys.*, *18*, 243–268.

Sleep, N. H. (1991), Hydrothermal circulation, anhydrite precipitation, and thermal structure at ridge axes, *J. Geophys. Res.*, *96*, 2375–2387.

Sohn, R. A. (2007), Stochastic analysis of exit-fluid temperature records from the active TAG hydrothermal mound (Mid-Atlantic Ridge, 26°N): 2. Hidden Markov models of flow episodes, *J. Geophys. Res.*, doi:10.1029/2007JB004961, in press.

Sohn, R. A., D. Fornari, K. L. Von Damm, J. A. Hildebrand, and S. C. Webb (1998), Seismic and hydrothermal evidence for a cracking event on the East Pacific Rise crest at 9°50′N, *Nature*, *396*, 159–161.

Sohn, R. A., J. A. Hildebrand, and S. C. Webb (1999), A microearthquake survey of the high-temperature vent fields on the volcanically active East Pacific Rise, *J. Geophys. Res.*, *104*, 25,367–325,378.

Temple, D. G., R. B. Scott, and P. A. Rona (1979), Geology of a submarine hydrothermal field, Mid-Atlantic Ridge, 26°N latitude, *J. Geophys. Res.*, *84*, 7453–7466.

Thompson, G., M. J. Mottl, and P. A. Rona (1985), Morphology, mineralogy, and chemistry of hydrothermal deposits from the TAG area, 26°N Mid-Atlantic Ridge, *Chem. Geol.*, *49*, 243–257.

Thompson, G., S. E. Humphris, B. Schroeder, M. Sulanowska, and P. A. Rona (1988), Active vents and massive sulfides at 26°N (TAG) and 23°N (SNAKEPIT) on the Mid-Atlantic Ridge, *Can. Mineral.*, *26*, 697–711.

Tivey, M. K., S. E. Humphris, G. Thompson, M. D. Hannington, and P. A. Rona (1995), Deducing patterns of fluid flow and mixing within the active TAG mound using mineralogical and geochemical data, *J. Geophys. Res.*, *100*, 12,527–512,555.

Tivey, M. K., A. M. Bradley, T. M. Joyce, and D. Kadko (2002), Insights into tide-related variability at seafloor hydrothermal vents from time-series temperature measurements, *Earth Planet. Sci. Lett.*, *2002*, 693–707.

Tivey, M. A., H. Schouten, and M. C. Kleinrock (2003), A near-bottom magnetic survey of the Mid-Atlantic Ridge axis at 26°N: Implications for the tectonic evolution of the TAG segment, *J. Geophys. Res.*, *108*(B5), 2277, doi:10.1029/2002JB001967.

Van Dover, C. L., B. Fry, F. J. Grassle, S. E. Humphris, and P. A. Rona (1998), Feeding biology of the shrimp *Rimicaris exoculata* at hydrothermal vents on the Mid-Atlantic Ridge, *Mar. Biol.*, *98*, 209–216.

Von Damm, K. L., C. M. Parker, and K. A. Beers (2005), The relationship of changes in the 9°50′N EPR hydrothermal system to observed seismicity: 2002–2004, *Eos Trans. AGU*, *86*(52), Fall Meet. Suppl., Abstract T31A-0492.

Wang, K., and E. E. Davis (1996), Theory for the propagation of tidally induced pore pressure variations in layered subseafloor formations, *J. Geophys. Res.*, *101*, 11,483–11,495.

Wichers, S., R. Reves-Sohn, and G. Terray (2005), New Constraints on the Thermal Power of the TAG Hydrothermal System and the Dynamics of the Water Column Plume, *Eos Trans. AGU*, *86*(52), Fall Meet. Suppl., Abstract OS33A-1466.

Wilcock, W. S. D., and J. R. Delaney (1996), Mid-ocean ridge sulfide deposits; evidence for heat extraction from magma chambers or cracking fronts?, *Earth Planet. Sci. Lett.*, *145*, 49–64.

You, C.-F., and M. J. Bickle (1998), Evolution of an active sea-floor massive sulfide deposit, *Nature*, *394*, 668–671.

Zonenshayn, L. P., M. I. Kuzmin, A. P. Lisitsyn, Y. A. Bogdanov, and B. V. Baranov (1989), Tectonics of the Mid-Atlantic rift valley between the TAG and MARK areas (26–24°N): Evidence for vertical tectonism, *Tectonophysics*, *159*, 1–23.

R. A. Sohn, Woods Hole Oceanographic Institution, Woods Hole, MA 02543, USA. (rsohn@whoi.edu)